AgPd and CuPd Catalysts for Selective Hydrogenation of Acetylene

Madelyn R. Ball [a†], Keishla R. Rivera-Dones [a], Elise B. Gilcher [a], Samantha F. Ausman [a], Cole W. Hullfish [a], Edgard A. Lebrón [a,b], James A. Dumesic [a] *

[a] Department of Chemical and Biological Engineering, University of Wisconsin-Madison, Madison, WI 53706, United States
[b] Department of Chemical Engineering, University of Puerto Rico-Mayagüez, Mayagüez, Puerto Rico, 00682
[†] Present address: School of Chemical and Biomolecular Engineering, Georgia Institute of Technology, Atlanta, GA 30332

* Corresponding Author: jdumesic@wisc.edu

Abstract

The selective hydrogenation of acetylene has been studied over AgPd and CuPd catalysts. Controlled surface reactions were used to synthesize these bimetallic nanoparticles on both TiO_2 and SiO_2 supports. Chemisorption measurements of the bimetallic catalysts indicate that Pd prefers to be on the nanoparticle surface with a Cu parent catalyst while Pd prefers to be subsurface with a Ag parent catalyst. From energy dispersive X-ray spectroscopy analysis, the composition of the nanoparticles is determined to be more uniform on the SiO_2 support compared to the TiO_2 support. X-ray absorption spectroscopy results indicate that, after reduction, the CuPd bimetallic catalysts have some Pd-Pd bonds but the average number of Pd-Pd bonds decreases after reaction. Infrared spectra of adsorbed CO show an increased fraction of isolated Pd species are present on the bimetallic catalysts compared to the monometallic catalysts. Adsorption of acetylene and ethylene, however, indicate adsorbed surface species that require contiguous Pd ensembles. These results suggest that the surface structure of the catalyst is highly dynamic and influenced by the gas environment as well as the support. The catalysts are active for the selective hydrogenation of acetylene in an ethylene-rich environment under mild conditions. Over all catalysts, the ethylene selectivity is greater than 92%, however improved selectivity is observed over the bimetallic catalysts compared to monometallic Pd catalysts. An ethylene selectivity of 100% is observed over the $CuPd_{0.08}/TiO_2$ catalyst. The highest acetylene conversion rate per gram of Pd is observed over the $CuPd_{0.02}/TiO_2$ catalyst, while the highest turnover frequency is found over the $AgPd_{0.64}/TiO_2$ catalyst. The bimetallic SiO_2-supported catalysts have lower rates than Pd/SiO_2 but still show improved selectivity. The combined characterization measurements and reaction kinetics studies indicate that the performance improvements of the bimetallic catalysts may be attributed to both electronic and geometric modification of Pd by the parent Cu or Ag metal.

Keywords

Bimetallic catalysts, palladium, silver, copper, hydrogenation, acetylene, Fourier transform infrared spectroscopy, X-ray absorption spectroscopy

Introduction

The selective hydrogenation of acetylene in ethylene-rich streams is used to purify ethylene prior to polymerization reactions.[1] Acetylene levels are usually around 1% in ethylene streams and must be decreased to less than 5 ppm to reduce deactivation of the polymerization catalysts.[2,3] This process can be operated in either a front-end or tail-end process, referring to the placement of the hydrogenation unit either before the de-methanizer unit or after the de-ethanizer unit, respectively.[4] The tail-end process is operated at lower partial pressures of hydrogen and involves feeds that contain less light hydrocarbons compared to the front-end process. This hydrogenation reaction is typically carried out using Ni- or Pd-based catalysts, due to their high activity while achieving selectivity to the desired ethylene.[4,5] Studies have shown that metals such as Cu or Au are also active and selective, while metals such as Pt or Ir give lower selectivities.[4] To identify a desirable catalyst for acetylene hydrogenation in the presence of ethylene, it is important to achieve high activity while also maintaining high selectivity and avoiding over-hydrogenation to ethane.[6] Acetylene hydrogenation proceeds via a Horiuti-Polanyi mechanism where acetylene is first hydrogenated to a vinyl intermediate, which is subsequently hydrogenated to the desired ethylene.[7] Unselective production of ethane can occur via hydrogenation of ethylene directly, or by hydrogenation of the vinyl intermediate to ethylidene followed by hydrogenation to ethane. Studies on acetylene hydrogenation over Pd catalysts over the past decades have been summarized in several review papers.[4,8–10]

Importantly, it has been reported that the selectivity of Pd-based catalysts can be improved by forming bimetallic catalysts with Pd and a group IB metal such as Ag, Au, or Cu, [6,11–15] with AgPd catalysts often used in industrial processes.[3,16] It is suggested that by forming these Pd alloys, the d-band center of the Pd is shifted and therefore favors the desorption rather than hydrogenation of ethylene.[17] As a result, extensive research has been carried out on various aspects of acetylene hydrogenation over bimetallic catalysts. Many studies have investigated the role of the Pd site structure on ethylene selectivity. Work by Tsapina et al. used X-ray absorption spectroscopy to study Pd-Ga, Pd-Zn, and Pd-Ag catalysts and found that the distance between neighboring Pd atoms was increased from 2.75 Å to between 2.82-2.99 Å for the bimetallic catalysts.[18] They hypothesized that this dilution of Pd atoms can prevent acetylene from adsorbing in a strong multisite mode and improve ethylene selectivity. Investigation of $CuPd/Al_2O_3$ catalysts by Leviness et al. determined that the addition of Cu to Pd increased the catalyst stability and ethylene selectivity while decreasing the catalyst activity.[19] This effect was attributed to Cu breaking up Pd-hydride phases and decreasing the contiguous Pd sites which can dissociatively adsorb acetylene and lead to the formation of C_{4+} species. A series of works by Anderson and coworkers has also investigated $CuPd/Al_2O_3$ catalysts, determining that Pd improves the activity of Cu catalysts by facilitating H_2 dissociation at low temperatures.[10,15,20]

Computational work has also investigated acetylene hydrogenation to identify the origin of high ethylene selectivity over bimetallic catalysts[7,17,21] and to identify potential new catalytic materials.[22] For PdIn alloy surfaces, the ethylene selectivity was predicted to be higher on surfaces with single atom Pd sites than on surfaces with Pd trimer sites, suggesting that when ethylene is adsorbed more weakly on single atom Pd sites it desorbs as a product rather than being further hydrogenated.[21] These calculations were supported by experimental studies over well controlled

PdIn single crystal surfaces, showing that over PdIn crystals with single atom Pd sites 92% ethylene selectivity was achieved, while Pd_3In crystals with Pd trimer sites achieved only 21% ethylene selectivity. Other work has developed a descriptor to determine the relative rates of hydrogenation and C-C coupling reactions with the aim of identifying metals that reduce oligomerization reactions.[17] 1,3-butadiene is the presumed precursor to further oligomers, and it was determined that its selectivity was lowest over Pt and Ir catalysts and increased over Rh, Pd, and Cu. This desired low selectivity to 1,3-butadiene needs to be balanced, however, with the acetylene hydrogenation activity and selectivity to ethylene. Weak adsorption of acetylene on the catalyst surface will decrease the barriers for both the desired selective hydrogenation of acetylene and the undesired coupling reactions.[17]

Other computational studies have focused on the mechanism of acetylene hydrogenation on both monometallic Pd and alloy catalysts. Work by Mei et al. determined by DFT and kinetic Monte Carlo simulations that the selective formation of ethylene proceeds through a key surface vinyl species, while the unselective formation of ethane can occur from over-hydrogenation of ethylene to ethane directly or hydrogenation of vinyl to form ethylidene.[7] Studies of the effects of coverage on Pd surfaces determined that adsorption energies decrease on a covered surface because of repulsive interactions.[23] Additionally, increasing the surface coverage is determined to decrease the barrier for acetylene hydrogenation to the vinyl intermediate, from 66 kJ/mol at 0.25 ML coverage to 50 kJ/mol at 0.33 ML coverage.[7] The presence of Ag on the surface is concluded to improve the catalyst performance by weakening adsorption energies of all intermediates which increases the rates for both desorption and hydrogenation. Furthermore, Ag reduces the presence of large Pd ensembles which are expected to be active for C-C bond breaking.[7] Although catalyst performance is suggested to be highly dependent on the reaction conditions,[9] these first principles

calculations provide important insights into the mechanism of acetylene hydrogenation over both Pd and AgPd catalysts.

Acetylene hydrogenation chemistry has also been widely studied in the surface science community, with spectroscopic studies of both adsorption and reactions informing understanding of the catalyst surface. It is important to note that many of these studies have been carried out on single crystal surfaces under UHV conditions, and therefore, although they provide invaluable information about surface species, the dependence on pressure and temperature may not be the same as for an industrially relevant catalyst. Work by Gates and Kesmodel investigated the adsorption of acetylene[24–26] and ethylene[25,27] on Pd(111) and Pd(100) surfaces through high resolution electron energy loss spectroscopy. These studies determined that at low temperatures (< 250 K) acetylene chemisorbs on the Pd surface, while upon heating, acetylene is converted to ethylidyne. Ethylene binds more weakly than acetylene to the surface and is also converted to ethylidyne around 300 K. Later studies by Tysoe and coworkers identified the formation of a vinylidene surface species formed after adsorption of acetylene on Pd(111) at room temperature and determined that the vinylidene species was stable up to 480 K.[28] Additional studies determined that the rate limiting step of acetylene hydrogenation is the addition of the first hydrogen to form the vinyl intermediate. It was also found that vinyl species can be converted to ethylidyne and that any surface vinylidene species can be hydrogenated to ethylidyne at high hydrogen pressures through a vinyl intermediate.[29] Computational studies have also informed the structure of surface species derived from acetylene and ethylene. Studies of adsorbed vinylidene on Pd(111) predict that acetylene can isomerize to vinylidene with a low barrier and that vinylidene is more stable than the starting acetylene.[30] Other calculations of vibrational spectra of adsorbed acetylene on Cu(111) and Pd(111) determined that the spectra are not sensitive to the particular adsorption site

(bridge or hollow) but are sensitive to the metal.[31] These studies indicate that a variety of surface species are present under acetylene hydrogenation conditions. As more direct evidence, recent work by Krooskwyk et al. investigated both surface and gas phase species during acetylene hydrogenation over a Pt(111) surface using polarization-dependent infrared spectroscopy. This work determined that, on a platinum surface, ethylidyne, ethylidene, and di-σ-bonded ethylene are all spectator species during acetylene hydrogenation.[32]

In this work, we have investigated AgPd and CuPd catalysts, synthesized by controlled surface reactions, for the selective hydrogenation of acetylene. By synthesizing catalysts with a measurable distribution of nanoparticle size and composition, we can develop structure-activity relationships for this system. The catalysts were characterized using STEM-EDS, CO chemisorption, and FTIR of adsorbed CO and adsorbed C_2H_4. In-situ FTIR studies of the catalysts under reaction conditions were used to identify surface spectator species. Although measuring the performance of acetylene hydrogenation catalysts at high conversion is important for industrial application,[4,8] in this work we focus on low conversion studies. This work aims to bridge the gap between adsorption on ideal surfaces and adsorption under reaction conditions on supported nanoparticle catalysts to understand the controlling factors for achieving high ethylene selectivity on AgPd and CuPd bimetallic catalysts.

Results and Discussion

Catalyst Synthesis

Ag and Cu parent catalysts were first prepared using deposition precipitation and ion exchange, respectively, on both TiO_2 and SiO_2 supports. Previous work has shown that the formation of bimetallic structures differs on TiO_2 and SiO_2 supports.[33] The metal loading,

determined by ICP, and the site densities, determined by N_2O titration, are shown in Table 1. Additionally, the average particle size, determined by STEM, is given for the parent catalysts. We note that although the Ag and Cu catalysts have different metal loadings, the metal particle sizes are similar for these catalysts.

Table 1. Metal loading as determined by ICP, CO uptake, and dispersion of bimetallic AgPd and CuPd catalysts and monometallic Pd catalysts

Catalyst	Ag wt%	Cu wt%	Pd wt%	(Ag/Cu):Pd (mol:mol)	CO uptake (μmol/g)	N_2O titration (μmol/g)	Dispersion (%)[a]	Average particle size (nm)
Ag/TiO_2	0.49	-	-	-	-	18.1	40	3.04 ± 1.67
Ag/SiO_2	0.32	-	-	-	-	16.0	54	1.99 ± 1.17
Cu/TiO_2	-	3.91	-	-	-	109	18	2.67 ± 1.29
Cu/SiO_2	-	4.15	-	-	-	131	20	4.34 ± 1.93
$AgPd_{0.64}/TiO_2$	0.28	-	0.17	0.64	1.6	-	10	2.04 ± 0.85
$AgPd_{0.15}/SiO_2$	0.43	-	0.06	0.15	4.8	-	84	1.96 ± 1.69
$CuPd_{0.08}/TiO_2$	-	4.12	0.56	0.08	16.6	-	32	1.90 ± 0.51
$CuPd_{0.02}/TiO_2$	-	4.46	0.15	0.02	5.5	-	39	1.63 ± 0.43
$CuPd_{0.09}/SiO_2$	-	4.93	0.75	0.09	22.2	-	31	2.81 ± 1.98
Pd/TiO_2	-	-	0.52	-	7.8	-	16	1.07 ± 0.30
Pd/SiO_2	-	-	0.50	-	4.3	-	9.2	1.72 ± 0.90

[a] Dispersion calculated using a stoichiometry of $N_2O + Ag_s \rightarrow Ag_sO + N_2$, $N_2O + 2Cu_s \rightarrow (Cu_s)_2O + N_2$, or 1Pd:1CO.

To synthesize the bimetallic catalysts, Pd was deposited by controlled surface reactions using cyclopentadienyl Pd allyl. The uptake of this precursor was monitored using UV vis spectroscopy of the solution. UV vis spectra shown in Figure 1 and Figure S1 indicate that the Pd precursor was taken up completely by the parent catalysts. Although Cp(Pd)allyl is partially deposited onto the TiO_2 and SiO_2 supports alone during control experiments,[33] additional uptake upon deposition onto the Ag and Cu catalysts indicates the formation of bimetallic particles. Furthermore, the uptake of Cp(Pd)allyl onto the support is linearly related to the concentration used,[33] and therefore using concentrations below 1 x 10^{-3} g Cp(Pd)allyl/g pentane in solution during synthesis reduces the uptake onto the support. The results described below indicate that although the uniformity of the nanoparticle composition varies between TiO_2 and SiO_2 supports,

detailed characterization enables the development of structure-performance relationships for these catalysts for acetylene hydrogenation.

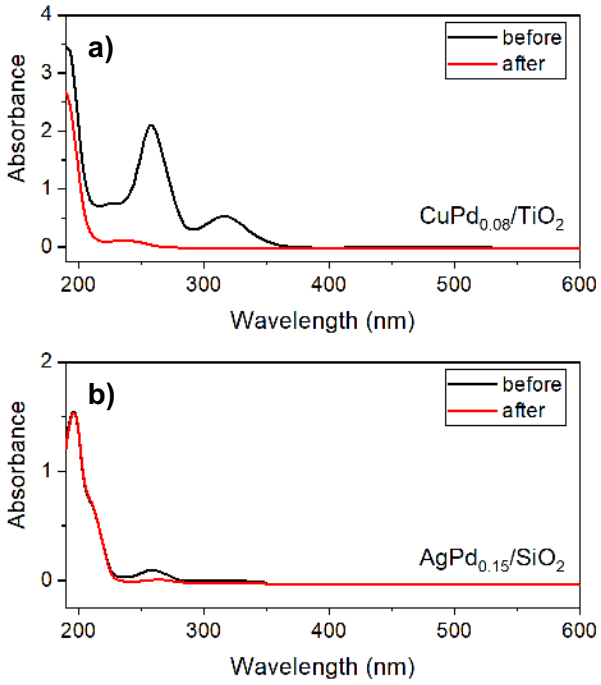

Figure 1. UV vis spectra showing the concentration of cyclopentadienyl Pd allyl in pentane, before (–) and after (–) mixing with the Ag or Cu parent catalyst in the synthesis of (a) $CuPd_{0.08}/TiO_2$, (b) $AgPd_{0.15}/SiO_2$.

Chemisorption and STEM analysis

The bimetallic catalysts were characterized using CO chemisorption to measure Pd dispersion. The metal loading of each catalyst, as determined by ICP, and the Pd dispersion calculated from CO uptake are shown in Table 1. The dispersions of all the CuPd catalysts, with molar ratios of Cu:Pd between 0.02 and 0.09, are between 30 and 40%. The AgPd catalysts, however, have a lower dispersion of 10% on the TiO_2 support and a higher dispersion of 84% on the SiO_2 support. This difference in dispersion between the Cu and Ag systems may be attributed to the differences in the relative surface and segregation energies for these two metal systems. For a CuPd alloy, the segregation energies under vacuum suggest that Pd has a slight preference to be

on the surface of Cu, while for a AgPd alloy, Pd prefers to be subsurface of the Ag.[34] In addition to the structural differences observed between the two parent metals, the catalyst support further enhances these differences. We anticipate the preference of Pd to be subsurface to be further enhanced on the partially reducible TiO_2 support as has been suggested for CuNi[35] and AuPd[36] systems. We note that the interaction between TiO_2 and the metal is likely not a partial overcoat as would be observed for strong metal support interactions (SMSI),[37,38] but an interaction of smaller magnitude. For the AgPd bimetallic catalysts, the stronger interaction between Pd and TiO_2, compared to Pd-Ag interactions, results in subsurface Pd, while on SiO_2, Pd remains on the surface of the bimetallic particles, as indicated by the higher dispersion. The lower dispersion for Pd/SiO_2 compared to Pd/TiO_2 may also be attributed to the weaker interaction between the Pd and SiO_2 support. Overall, the differences in dispersion and Pd surface structure for these CuPd and AgPd catalysts on SiO_2 or TiO_2 are influenced by the choice of both the parent metal and the support.

The composition distribution for the CuPd bimetallic catalysts was measured using STEM-EDS analysis. The electron beam was placed on individual nanoparticles and EDS spectra quantified to measure the relative amount of each metal. The composition distributions, along with representative TEM images, are shown in Figure 2. For both the $CuPd_{0.08}/TiO_2$ and $CuPd_{0.02}/TiO_2$ catalysts, the distribution is broad (average compositions of 55.7 ± 33.5 at% Pd and 37.6 ± 35.4 at% Pd, respectively), containing monometallic Cu as well as bimetallic CuPd particles of varied ratios. Some monometallic Pd nanoparticles are also present. This broad distribution of nanoparticle compositions suggests that there is also likely a broad distribution of surface composition and structures. In contrast, the $CuPd_{0.09}/SiO_2$ catalyst has a narrower distribution of particle compositions, with an average composition of 13.8 ± 10.9 at% Pd and most particles

containing less than 15 at% Pd. No monometallic Pd particles were detected for this catalyst. This narrow distribution indicates that the Pd surface structures on the SiO_2 supported CuPd catalyst are uniform across the catalyst. This may be due, in part, to the weaker interaction between Pd and the SiO_2 support and relatively stronger Pd-Cu interaction, compared to TiO_2, which reduces the formation of monometallic Pd moieties. We note that the close X-ray edge energies between Ag and Pd prevent a similar analysis on those catalysts.

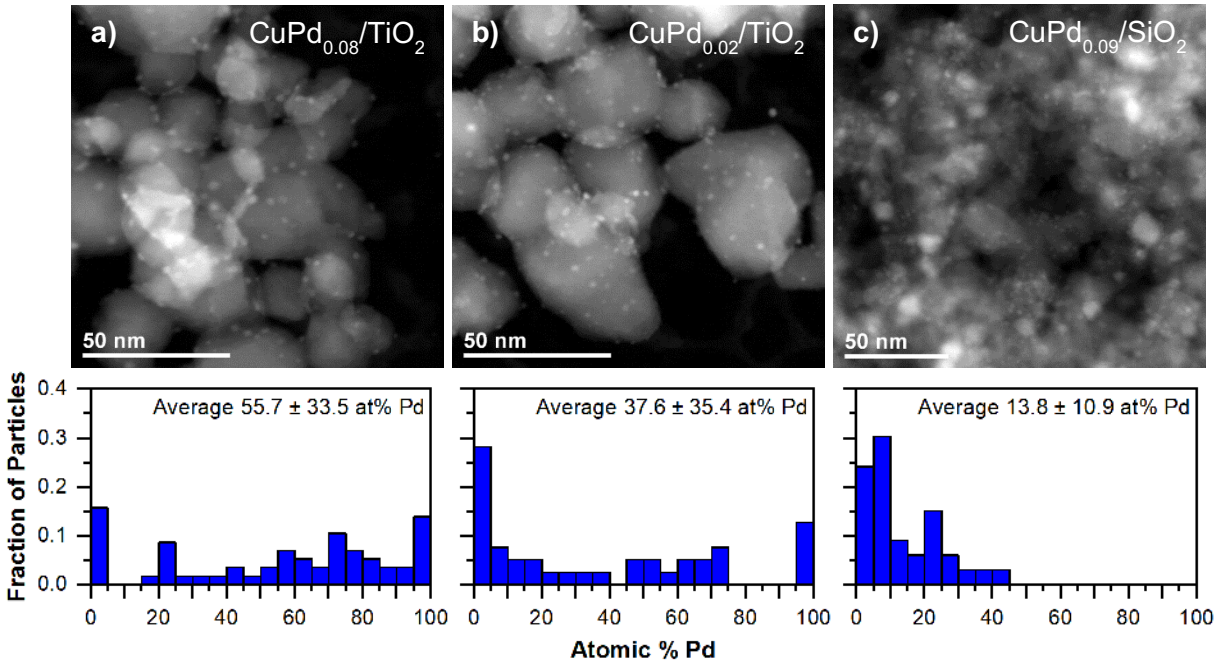

Figure 2. Representative STEM images (top) and nanoparticle composition distributions as determined by EDS analysis (bottom) for (a) $CuPd_{0.02}/TiO_2$, (b) $CuPd_{0.08}/TiO_2$, and (c) $CuPd_{0.09}/SiO_2$. For each composition distribution a minimum of 30 nanoparticles from multiple areas of the sample were analyzed.

X-ray absorption spectroscopy

X-ray absorption spectroscopy was used to identify changes to the metal coordination and oxidation state between the bimetallic systems and between catalyst pretreatments. From the X-ray near edge absorption spectra (XANES), it was determined that the catalysts were more easily

reduced on the TiO_2 compared to the SiO_2 support (Table 2). Additionally, the presence of Pd in the bimetallic catalysts further helps to reduce the Cu or Ag parent metal. McCue et al. have reported similar observations.[20] From XANES analysis at the Pd edge, the Pd is not fully reduced after treatment in H_2 at 473 K, with between 21 and 66% of the Pd remaining as PdO. After reaction, however, the fraction of metallic Pd in all of the catalysts increases, indicating that the metal is further reduced by the reaction mixture of hydrocarbons and hydrogen. This result is supported by the long activation time observed during reaction, requiring up to 24 hours for bimetallic catalysts to reach steady state. The XANES spectra are shown in Figures S3-S10.

Table 2. Oxidation state for Ag, Cu, Pd, and bimetallic catalysts from XANES fits at the Ag-K edge (25514 eV), Cu-K edge (8979 eV), and Pd-K edge (24350 eV). The fractional composition of metallic and oxide species is shown after the catalysts were treated (i) in He at room temperature (He), (ii) calcined at 723 K in 3% O_2 then reduced at 473 K in 3% H_2 (reduced), or (iii) after 24 hours reaction at 313 K (post reaction).

Catalyst		Ag_2O	Ag	CuO	Cu	PdO	Pd
Ag/TiO_2	He	0.17	0.83				
	Reduced	0.00	1.00				
Ag/SiO_2	He	0.23	0.77				
	Reduced	0.45	0.55				
Cu/TiO_2	He			0.97	0.03		
	Reduced			0.93	0.08		
Cu/SiO_2	He			0.76	0.24		
	Reduced			1.00	0.00		
$AgPd_{0.64}/TiO_2$	He	0.00	1.00			0.06	0.94
	Reduced	0.09	0.91			[a]	[a]
	Post reaction	0.00	1.00			0.00	1.00
$AgPd_{0.15}/SiO_2$	He	0.15	0.85			0.54	0.46
	Reduced	0.33	0.67			[a]	[a]
	Post reaction	0.34	0.66			0.40	0.60
$CuPd_{0.08}/TiO_2$	He			1.00	0.00	0.89	0.11
	Reduced			0.88	0.12	0.55	0.45
$CuPd_{0.02}/TiO_2$	He			1.00	0.00	1.00	0.00
	Reduced			0.62	0.38	0.57	0.43
	Post reaction					0.32	0.68
$CuPd_{0.09}/SiO_2$	He			0.95	0.05	0.89	0.11
	Reduced			0.46	0.54	0.56	0.44
	Post reaction					0.44	0.56
Pd/TiO_2	He					0.52	0.48
	Reduced					0.66	0.34
	Post reaction					0.17	0.83
Pd/SiO_2	He					0.18	0.82

Reduced	0.21	0.79
Post reaction	0.09	0.91

[a] Spectra for AgPd catalysts at Pd edge were too noisy for reliable fitting.

Extended X-ray absorption fine structure (EXAFS) analyses were carried out on these catalysts and the results are shown in Table 3 and Figures S11-S21. From the Pd edge, we observe that for the monometallic Pd catalysts, the total coordination number is lower for Pd/TiO_2 than for Pd/SiO_2. This finding would support the idea that the metal-TiO_2 interaction leads to some metal buried at the interface with the support, as discussed above. The $CuPd_{0.02}/TiO_2$ and $CuPd_{0.09}/SiO_2$ catalysts, without pretreatment (He) show no Pd-Pd coordination, indicating that the Pd is well dispersed in the Cu parent metal. Upon reduction of the catalyst, both the $CuPd_{0.02}/TiO_2$ and $CuPd_{0.08}/TiO_2$ catalysts show an increase in Pd-Pd coordination, while Pd-Pd scattering remains absent for the $CuPd_{0.09}/SiO_2$ catalyst. Thus, the catalyst structure changes more drastically for the TiO_2 supported catalysts after pretreatment and some Pd agglomeration occurs. For the AgPd catalysts, the close edge energies between the two metals make it such that Pd – Pd and Pd – Ag scattering (and the analogous scattering at the Ag edge) cannot be distinguished. Therefore, the total coordination is compared from each of the edges. The $AgPd_{0.64}/TiO_2$ catalyst before pretreatment (under He) has a higher coordination number from the Pd edge than from the Ag edge. This result indicates that the two metals have different average environments, and that Pd prefers to be subsurface and the surface is Ag enriched, in agreement with the chemisorption results above. This same catalyst after reaction, however, has a coordination number similar between the Pd and Ag edges, indicating that structural rearrangement has occurred and that some Pd has been brought to the surface. These EXAFS results highlight the dynamic nature of the catalyst and the changes in structure that occur under different gas environments.

Table 3. EXAFS fits for AgPd, CuPd, and Pd catalysts at the Ag-K edge (25514 eV), Cu-K edge (8979 eV), and Pd-K edge (24350 eV). The spectra were collected at room temperature in He after the catalysts were (i) treated in He at room temperature (He), (ii) calcined at 723 K in 3% O_2 then reduced at 473 K in 3% H_2 (reduced), or (iii) after 24 hours reaction at 313 K (post reaction).

Catalyst		Scatter Path[a]	CN[b]	R (Å)[c]	ΔE_0 (eV)[d]	σ^2 (Å^2)	R-factor
$AgPd_{0.64}/TiO_2$	He	Pd – M	9.3	2.80	2.42	0.007	0.022
		Ag – M	7.9	2.86	1.79	0.007	0.060
	Reduced	Ag – M	5.3	2.84	1.60*	0.007	0.075
	Post reaction	Pd – M	8.0*	2.84	-1.67*	0.007	0.089
		Ag – M	8.0	2.86	2.77	0.007	0.046
$AgPd_{0.15}/SiO_2$	He	Ag – M	4.7	2.80	0.005**	0.011	0.075
		Ag – O	0.4	2.23*			
	Reduced	Ag – M	6.0	2.78	-0.073	0.019	0.015
		Ag – O	1.3	2.17			
	Post reaction	Pd – M	7.5*	2.86	-4.79*	0.007	0.049
		Ag – M	5.2	2.77	0.074	0.017	0.028
		Ag – O	1.2	2.19			
$CuPd_{0.08}/TiO_2$	He	Pd – Pd	2.0	2.74	5.19**	0.007	0.081
		Pd – Cu	–	–			
		Pd – O	2.7	2.00			
		Cu – Cu	0.8	2.48	0.60**	0.007	0.035
		Cu – O	3.6	1.95			
	Reduced	Pd – Pd	6.3	2.57	10.77*	0.007	0.008
		Pd – Cu	0.5	1.99			
		Cu – Cu	4.2	2.54	3.59**	0.007	0.032
		Cu – O	2.0	1.86			
$CuPd_{0.02}/TiO_2$	He	Pd – Pd	–	–	7.80**	0.007	0.076
		Pd – Cu	0.7*	2.45			
		Pd – O	3.7	2.02			
		Cu – Cu	0.3	2.19	6.37**	0.007	0.008
		Cu – O	3.5	1.93			
	Reduced	Pd – Pd	4.8	2.55	8.03**	0.007	0.033
		Pd – Cu	0.8	1.98			
		Pd – O	–	–			
		Cu – Cu	5.7	2.53	2.98**	0.007	0.061
		Cu – O	2.1	1.83			
	Post reaction	Pd – Pd	2.7	2.99*	15.88*	0.007	0.017
		Pd – Cu	7.0	2.59			
		Pd – O	0.8	1.98			
$CuPd_{0.09}/SiO_2$	He	Pd – Pd	–	–	7.03*	0.007	0.046
		Pd – Cu	2.4	2.56			
		Pd – O	2.5	2.00			
		Cu – Cu	–	–	7.85*	0.007	0.006
		Cu – O	3.1	1.90			
	Reduced	Pd – Pd	–	–	9.14*	0.007	0.010
		Pd – Cu	5.5	2.55			
		Pd – O	0.6	1.97			
	Post reaction	Pd – Pd	–	–	13.50	0.007	0.007
		Pd – Cu	7.8	2.58			

		Pd – O	0.4	1.98			
Pd/TiO_2	He	Pd – Pd	4.0	2.74	-0.11	0.007	0.011
		Pd – O	2.7	1.79			
	Reduced	Pd – Pd	2.2	2.75	4.86**	0.007	0.076
		Pd – O	3.3	2.00			
	Post reaction	Pd – Pd	6.7	2.75	2.04	0.007	0.053
Pd/SiO_2	He	Pd – Pd	11.2	2.74	2.81	0.007	0.013
	Reduced	Pd – Pd	11.5	2.73	3.31	0.007	0.013
	Post reaction	Pd – Pd	10.6	2.77	4.10	0.007	0.013

[a] The first metal listed in the scatter path indicates the edge at which the EXAFS data was collected.
[b] Coordination number, uncertainty ± 0.8 or less, *uncertainty ± 1.2 or less
[c] Distance between the absorber and back scatterer, uncertainty ± 0.08 or less, *uncertainty ± 0.68 or less
[d] Uncertainty ± 1.2 eV, *Uncertainty ± 1.5 – 2, **Uncertainty ± 2 – 4.6

Infrared spectroscopy

CO Adsorption

FTIR spectra of adsorbed CO were used to determine the structure of the surface Pd on the monometallic Pd and bimetallic CuPd and AgPd catalysts. As shown in Figure 3, CO binds to CuPd catalysts in three main configurations at 223 K. The peaks at 2113 cm^{-1} (TiO_2 support) and 2130 cm^{-1} (SiO_2 support) are assigned to adsorption of CO on atop Cu sites,[39] and the intensity of this peak decreases upon addition of Pd to the Cu parent catalyst, indicating a decrease in the available surface Cu species. This peak is observed in spectra reported by Goodman and coworkers for CO adsorbed on copper films.[40] Other work has reported a similar decrease in peak intensity upon addition of a promoting metal to a copper catalyst, indicating a decrease in the accessible copper surface.[39] No CO adsorption is observed on Ag sites at 223 K.[41] In the spectra for CO adsorbed on $CuPd_{0.08}/TiO_2$ (Figure 3A), we observe a peak at 2057 cm^{-1} which can be assigned to CO linearly adsorbed to the top of Pd atoms[42] and a smaller broad peak at 1977 cm^{-1} which can be attributed to a combination of CO adsorbed on bridge and 3-fold Pd sites.[43,44] For $CuPd_{0.02}/TiO_2$, this bridge and 3-fold peak disappears and CO is adsorbed on atop Pd and atop Cu sites only. On the $AgPd_{0.15}/TiO_2$ catalyst, a peak at 2073 cm^{-1} is observed, corresponding to CO on atop Pd sites.

For comparison, the spectrum for CO adsorbed on monometallic Pd/TiO_2 is also shown. Although peaks for all three binding configurations for CO on Pd are present, the peak for CO adsorbed on atop sites is much smaller than the peaks for bridge and 3-fold adsorption. CO adsorption is more stable on bridge and 3-fold sites on Pd, and prefers these sites when they are accessible.[45,46] Therefore, the increase in the linear adsorption on the TiO_2-supported bimetallic catalysts, compared to monometallic Pd/TiO_2, indicates that Pd is present in primarily isolated species, diluted in the Cu or Ag nanoparticles. For the SiO_2 supported bimetallic catalysts, adsorption of CO on atop sites is observed at 2056 cm^{-1} and adsorption on 3-fold sites is observed at 1894-1889 cm^{-1}. $CuPd_{0.09}/SiO_2$ and Pd/SiO_2 also adsorb CO on bridge sites, indicated by peaks at 1956 cm^{-1} and 1992 cm^{-1}, respectively. The SiO_2 supported bimetallic catalysts have an increase in linear adsorption indicating some isolated Pd sites, but also have contiguous Pd sites. Additionally, on both SiO_2 and TiO_2 supports, the shift to lower wavenumbers for the peak for CO adsorbed on atop Pd sites on AgPd compared to monometallic Pd indicates greater electronic interaction between the Pd and parent metal, with the Pd gaining *d* electrons because of its higher electronegativity.[47] This effect is increased further for the CuPd catalysts, where the larger atomic radius of Pd causes an increase in adsorption energy as the Pd content increases.[48] From both the IR spectra and the chemisorption results described above, we observe that both the parent metal and the catalyst support influence the Pd structure.

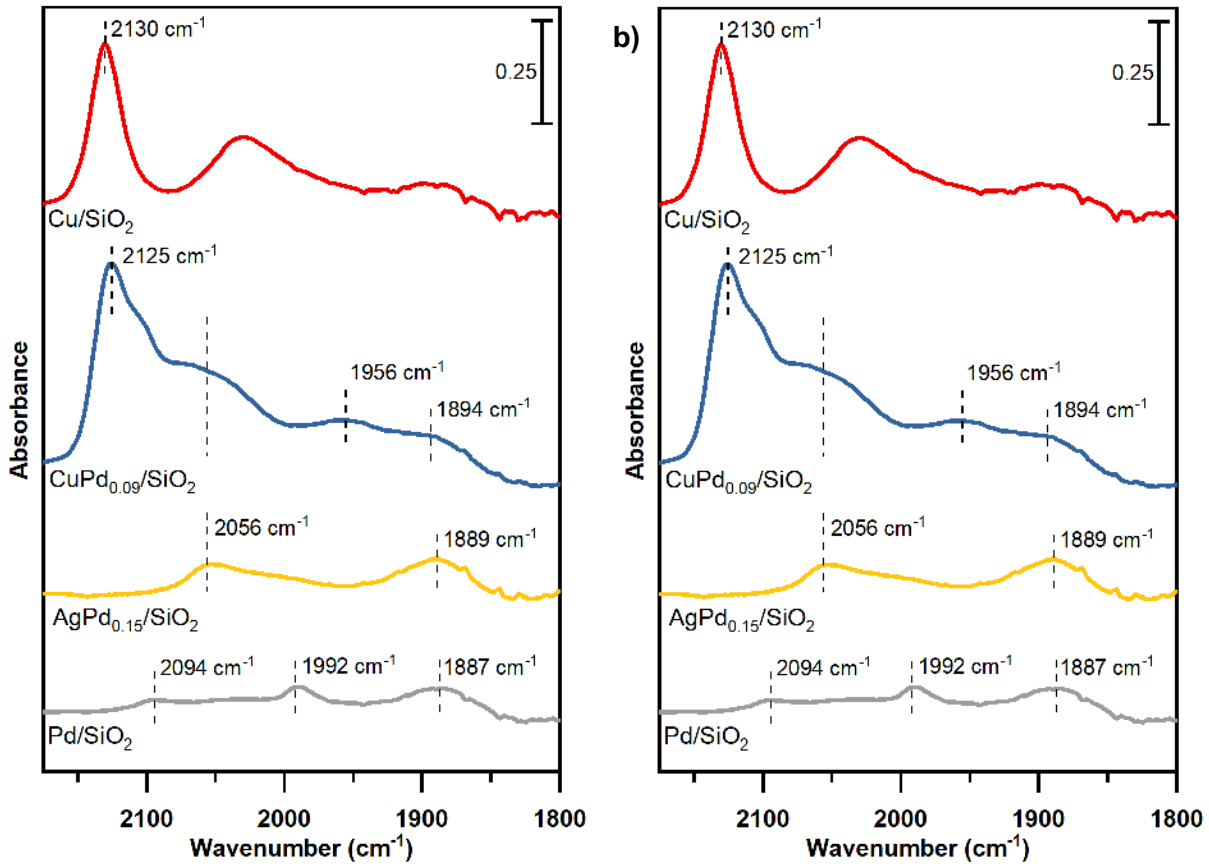

Figure 3. FTIR spectra of CO adsorbed on (a) TiO_2 supported catalysts and (b) SiO_2 supported catalysts. Monometallic Cu (red), monometallic Pd (gray), CuPd (green and blue), and AgPd (yellow) catalysts are shown. Catalysts were pretreated under H_2 at 473 K for 2 hours prior to adsorption of 300 Torr of 1% CO and spectra were collected at 223 K. Spectra were normalized by the pellet areal density and Pd containing catalysts were also normalized by site density as measured by CO chemisorption.

Ethylene adsorption

We investigated the adsorption of ethylene using infrared spectroscopy, since the nature of ethylene adsorption on the catalyst surface is hypothesized to be important in determining the selectivity during acetylene hydrogenation. For example, stronger adsorption of ethylene on the catalyst surface favors hydrogenation to ethane, while weaker adsorption of ethylene favors its desorption as a product.[49] The spectra in Figure 4 show the surface species formed after ethylene

adsorption on each of the catalysts once gas phase ethylene was removed from the cell. Three primary species have been reported on Pd/SiO_2 in the literature: ~1327 cm^{-1} for ethylidyne species, 1412 cm^{-1} for di-σ-bonded ethylene, and 1524 cm^{-1} for π-bonded ethylene.[50] The spectrum for Pd/SiO_2 shown in Figure 4B has a peak at 1415 cm^{-1} and a small peak at 1348 cm^{-1} which are assigned to di-σ-bonded ethylene and ethylidyne, respectively and a small amount of π-bonded ethylene is observed (peak at 1524 cm^{-1}). Comparing the spectrum for Pd/SiO_2 to the spectrum for Pd/TiO_2, we observe a similar ethylene adsorption mode and assign the peak at 1442 cm^{-1} to di-σ-bonded ethylene on Pd on a TiO_2 support. This blue shift of ~30 cm^{-1} indicates a weaker adsorption of ethylene on Pd/TiO_2, likely due to the increased Pd-TiO_2 interaction. This peak is also observed on the bimetallic $CuPd/TiO_2$ and $AgPd/TiO_2$ catalysts. These spectra indicate that after introducing ethylene to the catalysts and then removing gas phase ethylene, the remaining surface ethylene is adsorbed primarily in a di-σ configuration. There is a small peak at 1524 cm^{-1} on Pd/TiO_2 and $AgPd_{0.64}/TiO_2$, which corresponds to π-bonded ethylene. The addition of the π-bonded ethylene is expected as the surface becomes increasingly covered and only isolated Pd sites remain onto which ethylene can adsorb.[8] We also observe a π-bonded ethylene species bound to Cu at 1564 cm^{-1}.[51] The monometallic Pd catalysts and the AgPd catalysts form a small amount of ethylidyne on the surface (1351 cm^{-1}), while ethylidyne is not present on the CuPd bimetallic catalysts. On the SiO_2 support, the Cu, Ag, and bimetallic catalysts have negligible adsorption of ethylene or ethylene-derived surface species. This behavior indicates that ethylene adsorption on the bimetallic catalysts supported on SiO_2 is weaker than the corresponding TiO_2 supported catalysts. From chemisorption and EDS analysis, we know that the bulk and surface of these nanoparticles differ particularly between the TiO_2 and SiO_2 catalysts. These structural and compositional differences change the interaction between ethylene and the catalyst surface which is observed in these IR spectra. It is

important to note that removing the gas phase ethylene from the IR cell also allows weakly adsorbed surface species to desorb. Therefore, it is possible that other configurations or additional adsorbed ethylene are present under ethylene flow or reaction conditions but are removed upon purging the cell with inert gas.

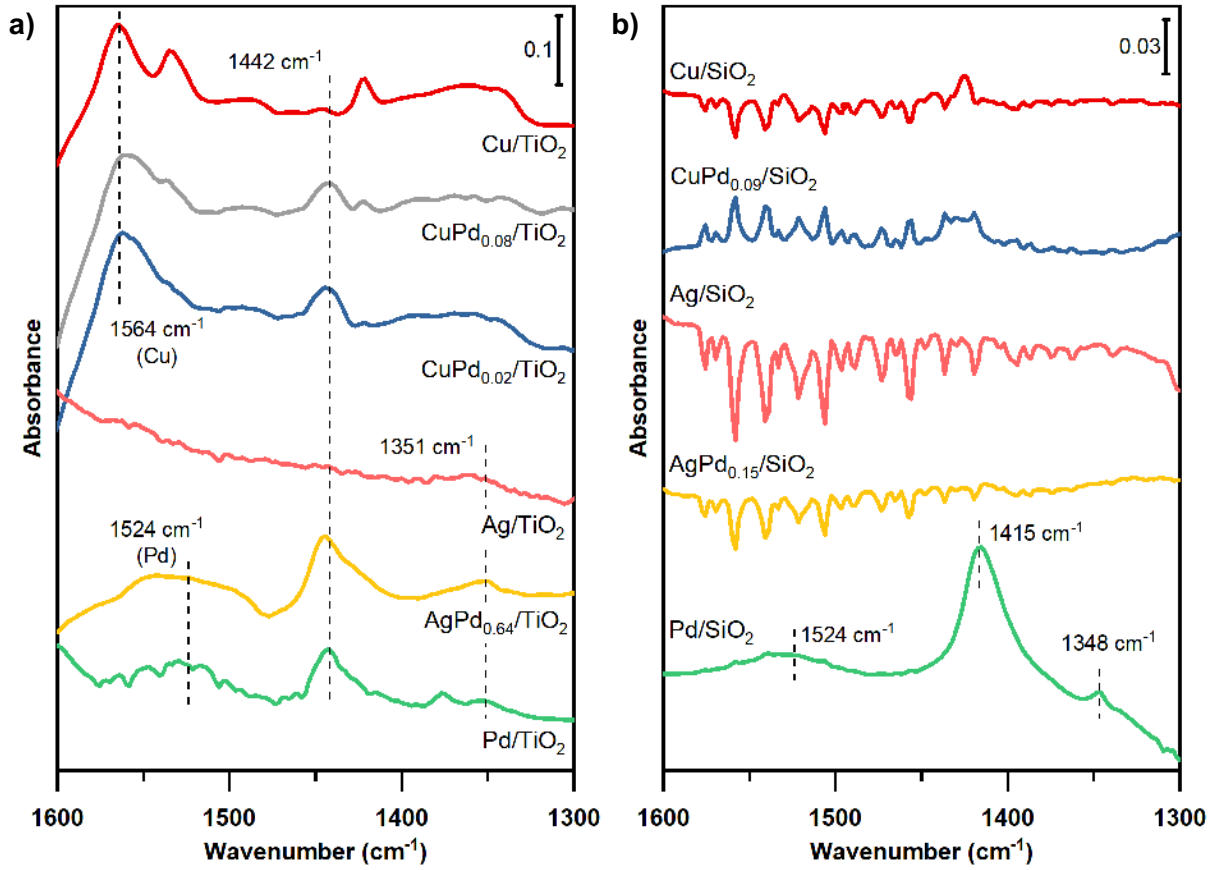

Figure 4. FTIR spectra of adsorbed ethylene on Cu (red), CuPd (gray and blue), Ag (pink), AgPd (yellow), and Pd (green) catalysts on (a) TiO_2 supports and (b) SiO_2 supports. All catalysts were reduced at 473 K under H_2 and cooled to 308 K for analysis. Monometallic Pd catalysts were purged with He at 473 K for 1 hour before cooling to avoid the formation of Pd hydride. The catalysts were exposed to flowing C_2H_4 for 30 minutes, then purged with He. The spectra shown represent the catalysts after He flow for 200 minutes and are normalized by the pellet areal density.

In situ infrared spectroscopy

In addition to ethylene adsorption, we carried out infrared spectroscopic studies of the catalysts after reaction flow to provide insight into the surface species present under catalyst operating conditions. First, a diluted reaction gas mixture was fed through the IR cell for longer than 2 hours to allow the catalyst to reach steady state, indicated by peak intensity no longer changing. The peaks from gas phase acetylene and ethylene around 3000 cm^{-1} and 1400 cm^{-1} mask any C-C or C-H stretches of surface hydrocarbon species, therefore, we incrementally remove the acetylene and ethylene to monitor changes due to desorption of these species and their derivatives.

Infrared spectra of the catalysts, after both acetylene and ethylene gas flows were stopped, are shown in Figure 5. We expect peaks corresponding to both gas phase and reactive surface species to disappear. The remaining observable species on the catalyst surface are strongly bound and expected to be spectator species under reaction conditions. It is known that the selective hydrogenation of acetylene on Pd catalysts runs on a highly covered surface and that the coverage influences the binding strength of intermediates.[16,52] Between 2800 and 3000 cm^{-1}, peaks attributed to CH stretches are observed. On the TiO_2 supported catalysts (Figure 5A), peaks for surface species at 2971 cm^{-1}, 2936 cm^{-1}, and 2871 cm^{-1} remain after the hydrocarbons are purged from the IR cell. These peaks are assigned to CH stretches in surface vinylidene and ethylidyne.[25,30] It has been reported that acetylene can isomerize to vinylidene which is more stable on Pd.[30] Additionally, on Pt surfaces, ethylidyne and di-σ-bonded ethylene have been observed as spectator species during acetylene hydrogenation.[32] These peaks have the largest intensity on the Pd/TiO_2 catalyst and the intensity decreases slightly on the $CuPd_{0.02}/TiO_2$ catalyst and further on $AgPd_{0.64}/TiO_2$. The intensities of analogous peaks on Pd/SiO_2 at 2982 cm^{-1}, 2951 cm^{-1}, 2924 cm^{-1}, and 2892 cm^{-1} are lower and then decrease further for peaks on the $CuPd_{0.09}/SiO_2$ catalyst at

2964 and 2932 cm^{-1} with a shoulder at 2858 cm^{-1}. These changes in peak intensity suggest that the bimetallic catalysts are less covered by ethylidyne and vinylidene spectator species than the monometallic Pd catalysts. Additionally, the similarity in peaks for these surface spectator species on $CuPd_{0.02}/TiO_2$ and Pd/TiO_2 suggests that this CuPd catalyst has structures similar to a monometallic Pd catalyst under these conditions. The differences between the SiO_2 and TiO_2 supported bimetallic catalysts are hypothesized to be due to the differences in the uniformity of the bimetallic nanoparticles, as shown by STEM-EDS analysis above. Additionally, we attribute differences between the supports to be due to the stronger Pd-TiO_2 interaction compared to Pd-SiO_2. The largest peak at 2971 cm^{-1} on Pd/TiO_2 suggests predominantly one surface species, likely ethylidyne, on interfacial sites between Pd/TiO_2,[13] while the similar peak areas for the peaks on Pd/SiO_2 indicate a wider range of surface species on Pd sites of varied coordination. On the Cu/TiO_2 and Cu/SiO_2 catalysts, there are small peaks in this same region suggesting that minimal amounts of ethylidyne and vinylidene species are formed on Cu sites.

Significant changes are also observed in the C-C stretching region between 1200-1500 cm^{-1} shown in Figure 5. The peaks at 1366 cm^{-1} and 1374 cm^{-1} are assigned to ethylidyne-type species on the support, and the peak at 1333 cm^{-1} is assigned to ethylidyne on Pd.[25,53] Peaks at wavenumbers higher than 1400 cm^{-1} are convoluted by species adsorbed on TiO_2 and SiO_2 (Figure S2) and therefore further deconvolution of the peaks to assign particular intermediates was not carried out. The range of 1400-1600 cm^{-1} includes adsorbed ethylene and acetylene, as well as vinylidene. Although the adsorption energy of acetylene is greater than the adsorption energy of ethylene,[24–27] the difference in concentration of these species in the feed likely leads to the presence of both species on the catalyst surface. The overall intensity of the peaks can be used to qualitatively measure the coverage of strongly adsorbed spectator species on the surface.

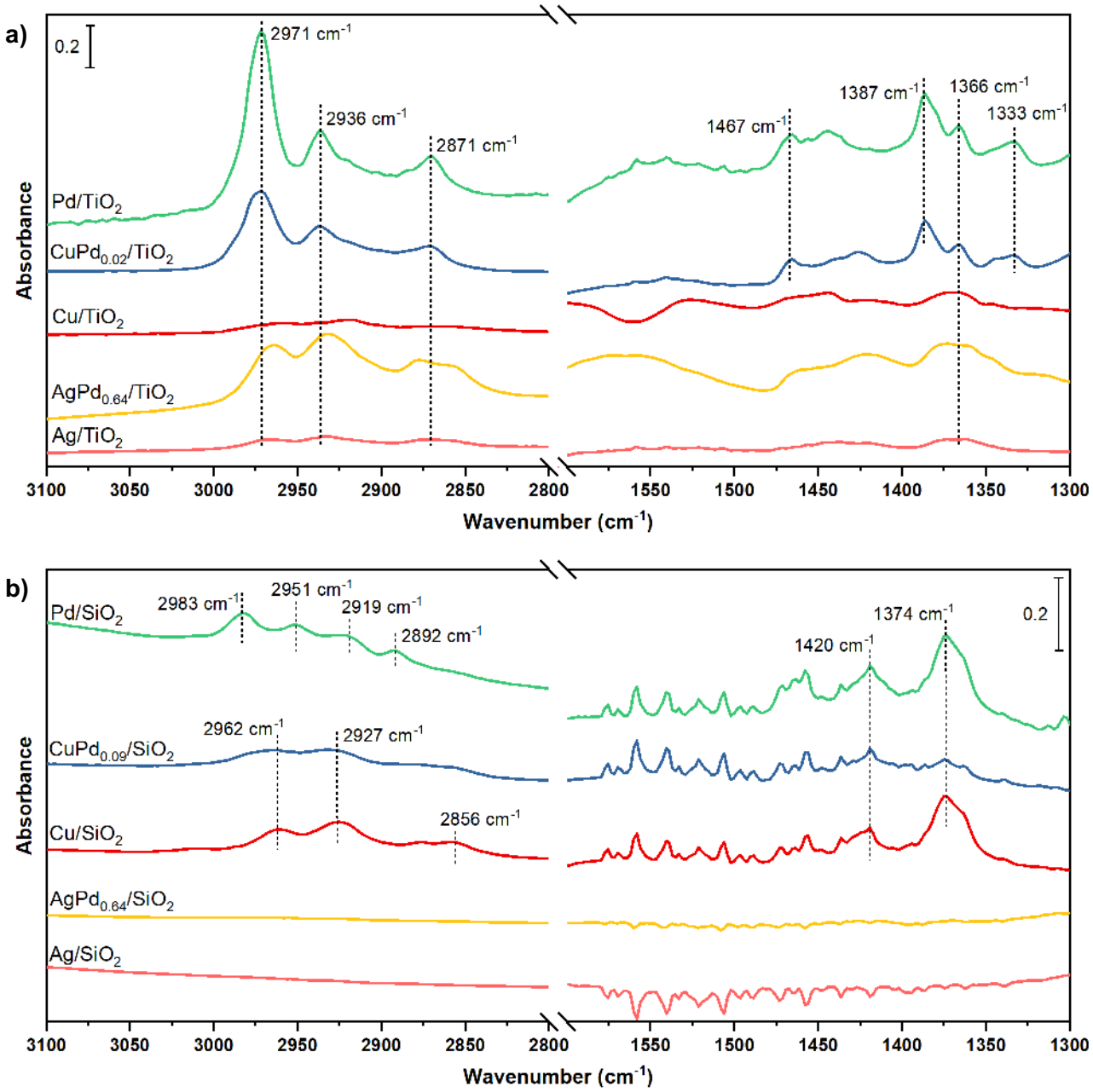

Figure 5. FTIR spectra of the TiO_2 (a) and SiO_2 (b) supported catalysts at 313 K after being exposed to reaction flow (0.083 bar C_2H_4, 0.003 bar C_2H_2, 0.083 bar H_2, balance Ar) for 2+ hours, under flow of C_2H_4 and H_2 for 2+ hours, then under flow of H_2 in Ar for 2+ hours. Spectra are normalized by the areal density of the catalyst pellet.

The peak intensities, both in the 2800-3100 cm^{-1} range and 1200-1600 cm^{-1} range, are lower for the CuPd and AgPd catalysts than for the monometallic Pd catalysts. This difference

indicates that the bimetallic nature of the CuPd and AgPd surfaces slightly decreases the presence of spectator species on the Pd surface. The SiO_2-supported catalysts have smaller peaks than the TiO_2 catalysts, particularly at the higher wavenumber range. This result suggests that the influence of the support is key in determining both the structure of the metal nanoparticle surface and, as a result, the coverage of the metal surface under reaction conditions. The large differences between the TiO_2 and SiO_2 supported catalysts may stem from the difference in nanoparticle composition and uniformity that we measured using STEM-EDS analysis, discussed above in Figure 2 as well as the interaction of the metal with the support. Additionally, for all catalysts, no changes were observed to the spectra upon removal of hydrogen to purge the IR cell with inert gas only.

Together, these characterization results indicate that both the support, TiO_2 or SiO_2, and the parent metal, Cu or Ag, influence the Pd structure. Specifically, the Pd dispersion is influenced by both support and parent metal; and, the highest dispersion is observed for $AgPd/SiO_2$ while the lowest dispersion is observed for $AgPd/TiO_2$. The CuPd catalysts on both supports have intermediate dispersions. The strength of interaction of hydrocarbon species with the surface is also influenced by both the support and the parent metal. The size of surface Pd ensembles and uniformity of nanoparticle composition are predominantly influenced by the support choice. With this information, it can be determined which properties most strongly influence catalytic performance.

Reaction Kinetics Studies

Acetylene hydrogenation reactions were carried out over these AgPd, CuPd, and Pd catalysts at 313 K and 1 atm. A molar ratio of 1:25:25 C_2H_2:C_2H_4:H_2 was used for all reactions. We define the ethylene selectivity as:

$$S_{C_2H_4} = 1 - \left(\frac{C_2H_6}{C_2H_{2\,feed} - C_2H_2} \right).$$

At acetylene conversions less than 2%, the monometallic Pd/TiO_2 catalyst is 95% selective to ethylene and the bimetallic catalysts supported on TiO_2 are more than 98% selective to ethylene, as shown in Figure 6A. Additionally, the Pd/SiO_2, $CuPd_{0.09}/SiO_2$, and $AgPd_{0.15}/SiO_2$ catalysts are 93%, 97%, and 97% selective to ethylene, respectively. These results indicate that the ethylene selectivity is enhanced by diluting the Pd in the Ag or Cu. This has been hypothesized to be due to a weakened binding of intermediates on the Pd sites in a bimetallic catalyst, as has previously been reported in both theory and experimental studies,[6,52,54] and is supported by our infrared spectra of adsorbed ethylene and reaction mixtures. The high selectivity achieved over the monometallic Pd catalysts can be attributed to the highly covered surface under reaction conditions. Previous studies have suggested that strongly bound species derived from acetylene and ethylene on Pd surfaces leaves only isolated Pd sites as active sites, resulting in high ethylene selectivity.[55,56] Additionally, surface vinylidene species observed in our infrared spectra have been suggested to be a precursor to the selective formation of ethylene.[57] Furthermore, the strong interaction between the metal nanoparticles and TiO_2 may lead to electronic effects which improve the ethylene selectivities compared to the SiO_2 supported catalysts. This result is in agreement with previous work that has shown enhanced ethylene selectivity for Pd/C compared to Pd/Al_2O_3 and Pd/MgO, attributed to metal-support interactions.[10,58] We note that for all catalysts studied, the carbon balance was closed to >99% and there were no observed C_{4+} species, as have been previously reported to form over Pd catalysts.[59] The IR spectra described above and the reactivity results together support the well-established Horiuti-Polanyi mechanism for the selective hydrogenation of acetylene.[7,9]

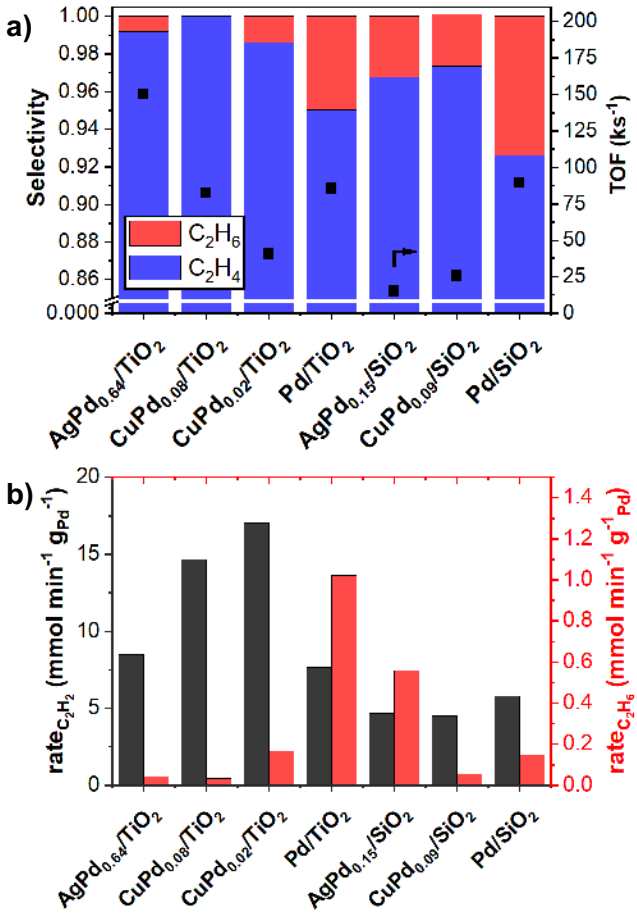

Figure 6. Catalytic performance for acetylene hydrogenation over AgPd, CuPd, and Pd catalysts. (a) Selectivities and turnover frequencies and (b) the rate of acetylene consumption (black, left axis) and ethane production (red, right axis) are shown. Acetylene conversions were below 3% for all reactions. Reaction conditions: 313 K, 1 atm, 150 sccm, feed composition: 1% C_2H_2, 25% C_2H_4, 25% H_2, balance He.

Under the conditions investigated in this work, the monometallic Pd and bimetallic CuPd and AgPd catalysts do not significantly deactivate over 12 hours of time-on-stream. The acetylene conversion turnover frequency (with sites counted by CO adsorption using 1 Pd:1 CO) as a function of time on stream is shown in Figure S22. The primary route for Pd catalyst deactivation during acetylene hydrogenation is hypothesized to be the formation of oligomeric species formed from C-C coupling reactions.[60,61] These species can form "green oil," blocking active sites and subsequently deactivating the catalyst. Our observed catalyst stability is in agreement with the

absence of C_{4+} products, detected by GC. The higher hydrogen pressures used in these reactivity studies, comparable to typical "front-end" acetylene hydrogenation conditions and low conversions likely limits the deposition of carbon on the catalyst surface.[52]

The turnover frequencies for acetylene consumption (with sites determined by CO adsorption) are shown in Figure 6A and the rates of acetylene conversion and ethane production per gram of Pd are shown in Figure 6B. The monometallic catalysts have higher rates of ethane production (Figure 6B, shown in red) than the bimetallic catalysts, although for all catalysts, the ethane production rate is much lower than the acetylene consumption rate (shown in black). Both the turnover frequency and the rate of acetylene conversion per gram of Pd are higher over the TiO_2 supported bimetallic catalysts than the SiO_2 supported bimetallic catalysts, which indicates that TiO_2 may be influencing the overall activity. In particular, comparing the activity of $CuPd_{0.08}/TiO_2$ and $CuPd_{0.09}/SiO_2$, which have similar ratios of Cu:Pd, metal loadings, and Pd dispersions, reflects the effect of TiO_2. Partially reducible supports have been previously reported to induce partial charge transfer between the support and metal nanoparticle. In this system, electron transfer from the TiO_2 support to the Pd may enhance the overall rate.[62,63] Previous studies have attributed an increase in Pd electron density to support basic sites; the weak basic sites on TiO_2 may contribute to this charge transfer.[64,65] Furthermore, the acidity of the TiO_2 support may contribute to enhanced activity due to promoted hydrogen spillover.[64] The support may also influence catalytic performance due to the differences in bimetallic nanoparticle structure; from the CO FTIR experiments, it is observed on the TiO_2 supported bimetallic catalysts that Pd is primarily isolated from other Pd species. The EDS analysis of these catalysts, which indicates that the $CuPd_{0.08}/TiO_2$ catalyst has a wide range of nanoparticle compositions, suggests that the Pd-rich or Pd-poor nanoparticles that are not found in the $CuPd_{0.09}/SiO_2$ catalyst contribute to enhanced

activity. Additionally, from ethylene and reaction mixture FTIR studies, more adsorbed hydrocarbons were observed on the TiO_2 supported catalysts, which may also be influencing the increased rate.

For the monometallic Pd/TiO_2 and Pd/SiO_2 catalysts, however, the rate and turnover frequencies are similar for the catalysts. This similarity is attributed to the similar nanoparticle structure for the monometallic catalysts and suggests that changes induced by the support are greater for the bimetallic catalysts than the monometallic Pd catalysts. Therefore, it is suggested that the rate enhancement observed for TiO_2 supported bimetallic catalysts is primarily due to structural changes to the nanoparticles, induced by the metal interaction with the support, and not from direct electronic modification of active sites by the support.

The highest rates of acetylene consumption per gram of Pd are observed on the $CuPd/TiO_2$ catalysts, and both the $CuPd_{0.08}/TiO_2$ and $CuPd_{0.02}/TiO_2$ catalysts have approximately the same rate. We also note that these $CuPd/TiO_2$ catalysts, in particular, offer high selectivity as well as high activity at low conversion, avoiding the tradeoff of decreased activity with an increase in selectivity as has been previously reported.[66] The rate of acetylene conversion over the $AgPd_{0.64}/TiO_2$ catalyst is at least 2 times lower than the rate over the $CuPd/TiO_2$ catalysts, however, the highest turnover frequency is observed for this $AgPd_{0.64}/TiO_2$ catalyst. The opposing trends for rates and turnover frequencies for these bimetallic, TiO_2 supported catalysts can be, in part, accounted for by the differences in surface sites. The lower number of surface sites, as measured by chemisorption, for the $AgPd/TiO_2$ catalyst leads to a higher TOF. The high ratio of Ag:Pd in this catalyst may facilitate intimate contact in the bulk between the two metals, while the lower dispersion for AgPd compared to the CuPd catalysts may prevent the formation of contiguous surface Pd sites which bind intermediates more strongly. It also been previously suggested for

CuPd catalysts that subsurface Pd may also contribute to the overall activity.[14] The ratio of the two metals likely also influences the observed activity trends. The decreasing TOF as the parent:Pd ratio decreases for the bimetallic TiO_2 catalysts indicates that the surface Pd is more active when there is more total Pd in each nanoparticle. This trend is likely due to charge transfer between the metals, improved reducibility of the parent metal, or other electronic modifications, as observed in the IR and XAS experiments.

The $CuPd_{0.08}/TiO_2$ catalyst has a TOF of 83 ks^{-1} followed by $CuPd_{0.02}/TiO_2$ and $CuPd_{0.09}/SiO_2$ with TOFs of 40 ks^{-1} and 25 ks^{-1}, respectively. The decrease in TOF over the CuPd bimetallic catalysts compared to the monometallic Pd catalysts may be due to weakened binding of reactive intermediates on the surface. Although this weakened binding may contribute to the increased selectivity, since ethylene will desorb rather than undergo further hydrogenation, it may also lead to decreased coverage of acetylene. Thus, the improved selectivity achieved on the CuPd bimetallic catalysts comes at a cost of decreased acetylene consumption turnover frequency. A similar decrease in catalytic activity was observed by Leviness et al. for $CuPd/Al_2O_3$ catalysts.[19] It is important to note, as indicated by the IR spectra of adsorbed CO and ethylene described above, the use of CO adsorption to measure the active sites may not be representative of the actual catalyst surface under reaction conditions. Thus, we use site densities derived from CO adsorption as a scaling factor to normalize rates and acknowledge that the catalyst surfaces may be subject to adsorbate induced reconstruction. Indeed, CO has been used both in catalyst pretreatment and as a co-feed to improve selectivity for acetylene hydrogenation. Co-feeding CO in front end reactors has been reported to improve ethylene selectivity by competing with ethylene for adsorption sites and thus facilitating ethylene desorption.[4] CO pretreatment of CuPd catalysts has been reported to increase the concentration of Pd surface species, which was observed to increase acetylene

conversion while decreasing ethylene selectivity.[67] It was found that Pd-Pd dimer species increased, suggesting an important role of isolated Pd surface sites in achieving high ethylene selectivity.

From the FTIR spectra of adsorbed ethylene and acetylene, a variety of surface species were observed. The peak intensity, however, was much higher on the TiO_2-supported catalysts than on the SiO_2 supported catalysts, suggesting different coverages of spectator species. Since the activities of these bimetallic catalysts are similar, this behavior indicates that the sites that are occupied by spectator species are likely not the same sites as those sites occupied by reactive intermediates. Additionally, we determined that the ethylene selectivity over the CuPd/TiO_2 and CuPd/SiO_2 catalysts are similar. The EDS analysis determined that the nanoparticle composition distribution for these catalysts are different – the TiO_2 supported samples having a broad distribution of nanoparticle compositions including monometallic Pd particles and the SiO_2 supported sample having a uniform nanoparticle composition distribution without monometallic Pd particles. From FTIR analysis of adsorbed CO, we determined that isolated Pd species are on the catalyst surface in the presence of CO but the ethylene adsorption spectra indicate that contiguous Pd species are likely present under those conditions. Therefore, at the low conversions investigated in this work, it can be concluded that isolated Pd sites are not required to achieve high ethylene selectivity, as was shown in previous work in our group for hydrodechlorination.[33] In the CuPd catalysts studied in this work, the surface Pd distribution is highly dependent on the conditions and adsorbates present. The enhanced selectivity and activity achieved over bimetallic AgPd and CuPd catalysts can be attributed to a combination of electronic interactions between the metals and geometric effects through the dilution of Pd. The role of electronic effects in the enhanced selectivity over bimetallic catalysts compared to monometallic Pd catalysts is supported

in the literature by reports of a shifted *d*-band in Pd alloys as well as expansion of the lattice spacing.[17,48] Previous studies have attributed improvements in performance for selective hydrogenation of acetylene over bimetallic catalysts to be due to geometric dilution of Pd sites.[10,68]

To further compare the performance of the monometallic Pd and bimetallic catalysts, the apparent activation energies were measured for the Pd/SiO_2 and $CuPd_{0.09}/SiO_2$ catalysts and are shown in Figure 7. The activation energy for the Pd/SiO_2 catalyst is 42 kJ/mol while the activation energy for the $CuPd_{0.09}/SiO_2$ is 63 kJ/mol. Similar activation energies of 40 kJ/mol for a Pd foil[69] and 60 kJ/mol for a $AgPd/K^+$-β-zeolite catalyst[13] have been reported. The rate per gram of Pd and turnover frequency over the Pd/SiO_2 catalyst are both higher than over the $CuPd_{0.09}/SiO_2$ catalyst, indicating a decreasing rate with increasing activation energy as expected. We note, however, that this increased activation energy is observed for the catalyst with increased ethylene selectivity. This result is in agreement with DFT calculated descriptors for ethylene selectivity, where catalysts with increased hydrogenation barriers favor desorption of ethylene as a product rather than further hydrogenation to ethane.[49] Future reaction kinetic studies of the TiO_2 supported bimetallic catalysts would provide further insights on the role of the support in the kinetics of acetylene hydrogenation over bimetallic catalysts.

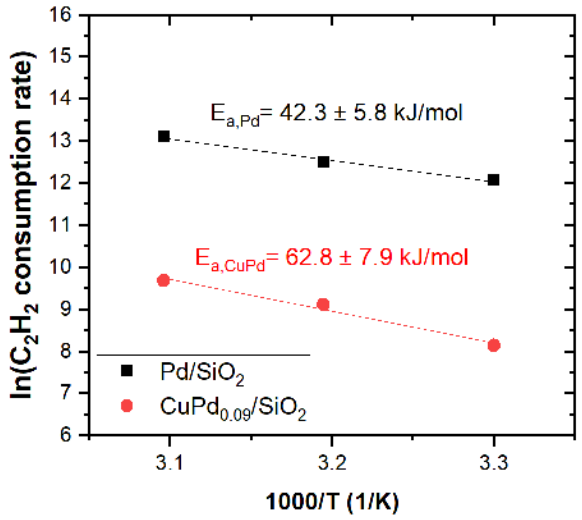

Figure 7. Arrhenius plot for Pd/SiO_2 (black square) and $CuPd_{0.09}/SiO_2$ (red circle) catalysts. Reaction conditions: 303-323 K, 1 atm, total flow 150 sccm, feed composition: 1% C_2H_2, 25% C_2H_4, 25% H_2, balance He.

Conclusions

In this work, an improved selectivity towards ethylene has been demonstrated during acetylene hydrogenation at low conversion over CuPd and AgPd catalysts, compared to monometallic Pd catalysts. The CuPd bimetallic catalysts are more than 99% selective for the desired hydrogenation to ethylene, while monometallic Pd catalysts were less than 95% selective to ethylene. $CuPd/TiO_2$ catalysts give the highest rate on a per Pd basis, while the bimetallic $AgPd/TiO_2$ catalyst gives the highest TOF. Thus, the change in the Pd surface structure achieved by forming bimetallic CuPd nanoparticles improves the selectivity to ethylene and improves the dispersion of Pd, but the rate per surface Pd is decreased. FTIR spectra of adsorbed CO indicate that Pd is isolated from other Pd species on the CuPd nanoparticle surfaces; however, the spectra of adsorbed ethylene indicate a di-σ binding configuration which requires neighboring Pd atoms. FTIR spectra of the catalysts after exposure to reaction conditions suggest that both electronic and geometric effects lead to the enhanced selectivity for AgPd and CuPd catalysts for selective

hydrogenation of acetylene. Additionally, the role of the support was investigated, and better performance was observed over the bimetallic catalysts supported on TiO_2 compared to SiO_2. This effect is attributed to structural and electronic effects, where the TiO_2 supported catalysts have isolated Pd species and higher coverages of hydrocarbons. These results indicate the role of both the parent metal and the support in enhancing catalytic performance for acetylene hydrogenation over Pd-based bimetallic catalysts.

Materials and Methods

Catalyst Synthesis

Fumed silica (Cabosil EH5) was acid washed prior to use. Approximately 15 g were added to ~1 L 0.1 M HNO_3 and the slurry was mixed for 2 hours. The silica was then filtered and washed with 18 MΩ MilliQ water, then dried in air at 383 K overnight. Once dry, the silica was crushed and sieved to between 60 and 100 mesh. Titania (Degussa P25) was used as received.

Ag/SiO_2 and Ag/TiO_2 catalysts were synthesized by deposition precipitation. The desired amount of silver nitrate ($AgNO_3$) (99+%, Sigma-Aldrich) in 18 MΩ MilliQ water was added to a slurry of SiO_2 or TiO_2 and was heated to 353 K. 0.1 M NaOH was added to adjust the pH of the slurry to 9 then stirred for 2 h. The catalyst was filtered and washed with excess water then dried at 383 K for 12 h. The Ag catalyst was then reduced at 623 K in H_2 (Industrial Grade, Airgas) for 6 h (heating rate 1.5 K/min). After cooling to room temperature, the catalyst was passivated in 1% O_2 in He (Airgas).

The parent Cu/TiO_2 and Cu/SiO_2 catalysts were synthesized using ion exchange. The desired amount of tetraammine copper sulfate ($[Cu(NH_3)_4]SO_4 \cdot xH_2O$, Strem) was added to 18 MΩ MilliQ water. A 5% ammonium hydroxide (NH_3OH, Sigma-Aldrich) solution was added to the copper solution to dissolve. Separately, either the TiO_2 or the SiO_2 was added to 18 MΩ water and

then the copper solution was added to the slurry. 2 M sulfuric acid (H_2SO_4, Sigma-Aldrich) was added to adjust the pH to 9. The slurry was stirred overnight then filtered and washed with excess water. The final catalyst was dried in a 333 K vacuum oven overnight. The dried Cu catalyst was treated first for 30 min at 573 K under Ar (Industrial Grade, Airgas) flow (heating rate 5 K/min) then at 673 K for 3 h under H_2 flow (heating rate 5 K/min). The catalyst was held at 673 K for an additional hour under Ar flow before cooling to room temperature and passivating in 1% O_2 in He.

Bimetallic CuPd and AgPd catalysts were synthesized using controlled surface reactions, a method developed in previous work for other multimetallic systems.[70–74] The general procedure is shown in Figure 8 below.

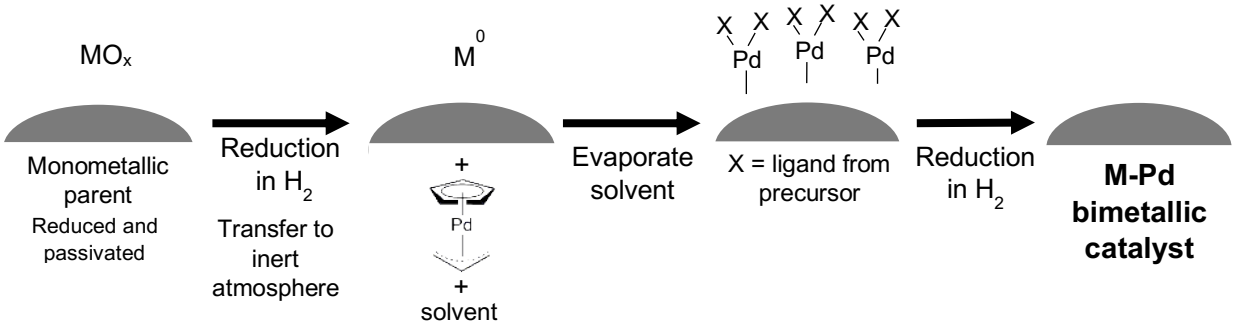

Figure 8. Schematic of controlled surface reaction approach to synthesizing supported bimetallic catalysts. The parent metal is denoted as M. Pd is deposited using a cyclopentadienyl Pd allyl organometallic precursor.

A portion of the parent catalyst, synthesized as described above, was reduced in H_2 for 4 h (heating rate 5 K/min) at 673 K for Ag and 573 K for Cu then cooled to room temperature and purged with inert gas. The catalyst was then sealed and transferred to an inert atmosphere glove box (Vacuum Atmospheres) using Schlenk techniques. The desired amount of cyclopentadienyl palladium allyl (Cp(Pd)allyl, 98%, Strem Chemicals) was dissolved in anhydrous *n*-pentane (≥99%, Sigma Aldrich) and then added to the Schlenk tube containing the parent catalyst. The slurry was stirred for 1 hour, then the catalyst was allowed to settle and a small portion of the

solution was removed for UV vis analysis. The remaining pentane was evaporated using Schlenk techniques and then the catalyst was reduced in flowing hydrogen at 673 K for 4 h (heating rate 5 K/min) without exposure to air. After reduction, the final catalysts were passivated in 1% O_2 in He. The bimetallic catalysts are designated MPd_x/support where M is the parent metal and x is the atomic Pd/M ratio as measured by inductively coupled plasma-optical emission spectroscopy.

For comparison, monometallic Pd/TiO_2 and Pd/SiO_2 catalysts with a loading of 0.5 wt% Pd were synthesized using incipient wetness impregnation. An aqueous solution of palladium nitrate hydrate ($Pd(NO_3)_2$, 40% Pd basis, Sigma Aldrich) was added dropwise to the support (TiO_2, C, or SiO_2) and continuously mixed until the incipient wetness point was reached. The catalyst was dried at 383 K in air overnight, reduced under flowing hydrogen at 533 K for 6 hours (with heating rate of 1 K min^{-1}), and then passivated with flowing 1% O_2 in He.

Characterization

Adsorption measurements

Surface Ag sites were measured using N_2O titration, following the methods of Seyedmonir et al.[75] Catalysts were reduced at 473 K in H_2 for 6 h (heading rate 0.75 K/min) and then evacuated to 10^{-5} Torr. N_2O was introduced to the catalyst samples at 443 K and oxidized the Ag surface by the following stoichiometry $N_2O + Ag_s \rightarrow Ag_sO + N_2$, where *s* represents a surface atom. Surface Cu sites were also measured using N_2O titration, following the methods of Evans et al.[76] Catalysts were reduced at 473 K in H_2 for 6 h (heating rate 0.75 K/min), evacuated to 10^{-5} Torr, and then N_2O was introduced to the sample at 363 K. The Cu surface was oxidized by the following stoichiometry $N_2O + 2Cu_s \rightarrow (Cu_s)_2O + N_2$. N_2O (CP Grade, Matheson) was purified by passing over Drierite prior to use. The pressure of N_2 was determined using a Baratron pressure gauge after condensing the remaining N_2O in a liquid nitrogen trap.

The Pd dispersion was measured by CO (CP Grade, Airgas) chemisorption using a custom volumetric and gas-handling apparatus. CO was purified by passing over copper turnings at 503 K to remove metal carbonyls and 4 Å molecular sieves to remove water prior to use. Catalyst samples were reduced in flowing hydrogen (Industrial Grade, Airgas) at 473 K for 6 h (heating rate 0.75 K/min) prior to analysis. After reduction, the samples were evacuated to 10^{-5} Torr and cooled to room temperature to collect the isotherms. CO adsorption was carried out at 293 K and the catalyst sample was evacuated for 30 minutes between collection of the first and second isotherms. The Pd site density is reported as the irreversible CO uptake using a stoichiometry of 1 Pd:1 CO.

Fourier transform infrared spectroscopy

Infrared spectra of probe molecules adsorbed on catalyst samples were collected using a Nicolet 6700 spectrometer connected to a custom vacuum manifold. Catalyst samples were pressed into self-supporting pellets and loaded into a transmission cell described elsewhere.[77,78] Prior to analysis, the samples were reduced in H_2 (Industrial Grade, Airgas) for 4h at 473 K (heating rate 5 K/min). For all experiments, spectra were collected with a resolution of 4 cm^{-1} spectra were normalized by the pellet area density (pellet area/pellet mass).

For CO adsorption experiments, the cell was evacuated to 10^{-5} Torr after reduction and then a background spectrum was collected at room temperature under vacuum. Then, 300 Torr of 1% CO (Airgas) was introduced to the cell and equilibrated for 10 minutes. The cell was then cooled to 103 K and equilibrated for an additional 10 minutes. The cell was evacuated to remove weakly adsorbed CO and spectra were collected at the desired temperature as the cell was allowed to warm.

For ethylene adsorption experiments, the cell was held at 308 K and purged with Ar after reduction. A background was collected and then ethylene (2.5 Grade, Praxair) was flowed through the cell for 30 minutes. Then, the cell was purged with Ar and spectra were collected.

For in situ experiments under reaction conditions, the cell was purged with Ar (UHP, Airgas) after reduction and the cell was cooled to 313 K. A background was collected in Ar and then the reaction mixture of 0.083 bar C_2H_4, 0.003 bar C_2H_2 (Airgas), 0.083 bar H_2 (Airgas), and balance Ar was fed to the cell. After collecting spectra for 2+ hours, the acetylene flow was stopped. After collecting spectra for an additional 2+ hours under C_2H_4, H_2, and Ar flow, the ethylene flow was stopped. Spectra were collected under H_2 and Ar flow, and then under Ar only.

For all FTIR spectra, comparisons between Pd containing catalysts were made with spectra normalized by the Pd site density in addition to the catalyst pellet areal density.

Inductively coupled plasma-optical emission spectroscopy

The total metal content of catalysts was determined using a Varian Vista-MPX CCD Simultaneous inductively coupled plasma-optical emission spectrometer (ICP-OES). Calibrations for ICP analysis were obtained by analyzing dilutions of commercial ICP standards (Fluka, 1000 mg L^{-1}).

UV-visible absorption spectroscopy

UV-visible absorption spectra of cyclopentadienyl Pd allyl in *n*-pentane were collected using a Thermo Scientific Evolution 300 UV-visible spectrometer. Spectra were collected over wavelengths ranging from 190 to 600 nm using a 1 cm path-length quartz cuvette to contain the samples. Solutions were prepared inside an inert glove box and then transferred to the cuvette in air for analysis. A control experiment using a sealed cuvette which was loaded in the glove box

and then analyzed without exposing the solution to air showed the same spectra as the same solution exposed to air to transfer to a cuvette, indicating negligible decomposition of the Cp(Pd)allyl precursor.

Scanning transmission electron microscopy – energy dispersive X-ray spectroscopy

Scanning transmission electron microscopy (STEM) imaging was performed using a FEI Titan STEM with Cs aberration correction operated at 200 kV in high-angle annular dark field (HAADF) mode. Energy dispersive X-ray spectroscopy (EDS) data was collected on the CuPd catalysts using the same microscope with an EDAX SiLi detector. Similarity between X-ray edges for Ag and Pd prevented similar analysis on those catalyst samples. Particle composition distributions of each sample were determined by EDS analysis of at least 30 particles. Samples were prepared by dropping the passivated catalyst, suspended in ethanol, on a holey carbon coated Cu grid. For EDS analysis of Cu-containing samples, holey carbon coated Au grids were used. The samples were plasma cleaned before loading in the microscope.

X-ray absorption spectroscopy

X-ray absorption spectroscopy measurements were carried out at beamline 10-ID at the Advanced Photon Source at Argonne National Lab. Spectra were collected at the Ag-K edge (25514 eV), Cu-K edge (8979 eV), and Pd-K edge (24350 eV). Catalysts were loaded into a stainless steel sample holder and pressed into self-supporting pellets. This sample holder was loaded into a quartz tube, sealed with fittings holding Kapton windows and treated at the relevant temperature and gas conditions. Data fitting was carried out using the Demeter package over an R range of 1.6 -3.6 Å and a k-range of 2.8 – 12.3 $Å^{-1}$ at the Ag edge, R range of 1.1-2.8 Å and a k-range of 2.4 – 10.8 $Å^{-1}$ at the Cu edge, and an R range of 1.1-2.8 Å and a k-range of 2.4 – 11.6 $Å^{-1}$ at the Pd edge.

The amplitude reduction factor was determined to be $S_0^2 = 0.74$ for Cu, $S_0^2 = 0.89$ for Ag, and $S_0^2 = 0.86$ for Pd, calculated from the spectra of the reference foils.

Reaction Kinetics Measurements

Catalysts were diluted in silica gel (Davisil Grade 646, 35-60 mesh, Sigma-Aldrich) then loaded into a ½-inch outer diameter, 304 stainless steel reactor between quartz wool (Ohio Valley Specialty) and silica chips (Sigma-Aldrich) for activity testing. The reactor was heated with a furnace (Applied Test Systems) and aluminum blocks were placed around the reactor to ensure isothermal operation. The temperature was controlled using a PID controller (Love Controls) with a K-type thermocouple placed between the aluminum block and used for temperature control. He (Industrial Grade, Airgas), H_2 (Industrial Grade, Airgas), C_2H_4 (CP Grade, Airgas), and C_2H_2 (Industrial Grade, Airgas) were delivered by mass flow controller (Brooks 5890E) and used without further purification. Prior to reaction, the catalyst bed was calcined in air (Breathing Air, Airgas) at 723 K for 90 minutes (heating rate 10 K/min) and then reduced in H_2 (Industrial Grade, Airgas) at 473 K for 3 hours. This pretreatment procedure was observed to improve the catalyst initial activity and reduce the activation time needed for steady state to be achieved. The reactor was purged with inert gas at 473 K for at least 30 minutes then cooled to reaction temperature (typically 313 K). Reactant and product analyses were performed by Shimadzu GC-2014 with He carrier gas using an FID detector and an RT Alumina Bond column for analysis of ethane, ethylene, and acetylene. All measurements were carried out at an acetylene conversion of less than 3% for rate measurements and less than 7% for kinetics measurements. The rate and selectivity values represent averages over 10 hours time on stream. The activation energy and reaction order measurements were taken after the catalyst was exposed to reaction flow for 24 hours and allowed to stabilize. The carbon balance for all reactions was >99%.

Supporting Information

UV vis spectra during catalyst synthesis, FTIR spectra of TiO_2 and SiO_2 supports after reaction mixture adsorption, XANES and EXAFS spectra, and reaction time on stream data for acetylene conversion

Acknowledgements

This material is based upon work supported by the US Department of Energy, Office of Basic Energy Sciences (DE-SC0014058). The authors gratefully acknowledge use of facilities and instrumentation at the UW-Madison Wisconsin Centers for Nanoscale Technology (wcnt.wisc.edu) partially supported by the NSF through the University of Wisconsin Materials Research Science and Engineering Center (DMR-1720415). This research used resources of the Advanced Photon Source, a U.S. Department of Energy (DOE) Office of Science User Facility operated for the DOE Office of Science by Argonne National Laboratory under Contract No. DE-AC02-06CH11357. MRCAT operations are supported by the Department of Energy and the MRCAT member institutions.

References

(1) Guo, Z.; Liu, Y. Y.; Liu, Y. Y.; Chu, W. *Appl. Surf. Sci.* **2018**, *442*, 736–741.

(2) Derrien, M. L. *Selective Hydrogenation Applied to the Refining of Petrochemical Raw Materials Produced by Steam Cracking*; Elsevier Science Publishers B.V., 1986; Vol. 27.

(3) Nguyen Thanh, C.; Didillon, B.; Sarrazin, P.; Cameron, C. Selective hydrogenation catalyst and a process using that catalyst. US 6054409, 2000.

(4) Borodziński, A.; Bond, G. C. *Catal. Rev.* **2006**, *48*, 91–144.

(5) Gannon, R. E.; Manyik, R. M.; Dietz, C. M.; Sargent, H. B.; Thribolet, R. O.; Schaffer, R. P. In *Kirk-Othmer Encyclopedia of Chemical Technology*; John Wiley & Sons, Inc.: Hoboken, NJ, USA, 2003.

(6) Pei, G. X.; Liu, X. Y.; Yang, X.; Zhang, L.; Wang, A.; Li, L.; Wang, H.; Wang, X.; Zhang, T. *ACS Catal.* **2017**, *7*, 1491–1500.

(7) Mei, D.; Neurock, M.; Smith, C. M. *J. Catal.* **2009**, *268*, 181–195.

(8) Borodziński, A.; Bond, G. C. *Catal. Rev.* **2008**, *50*, 379–469.

(9) Bos, A. N. R.; Westerterp, K. R. *Chem. Eng. Process. Process Intensif.* **1993**, *32*, 1–7.

(10) McCue, A. J.; Anderson, J. A. *Front. Chem. Sci. Eng.* **2015**, *9*, 142–153.

(11) Zea, H.; Lester, K.; Datye, A. K.; Rightor, E.; Gulotty, R.; Waterman, W.; Smith, M. *Appl. Catal. A Gen.* **2005**, *282*, 237–245.

(12) Zhang, Y.; Diao, W.; Williams, C. T.; Monnier, J. R. *Appl. Catal. A Gen.* **2014**, *469*, 419–426.

(13) Huang, W.; Pyrz, W.; Lobo, R. F.; Chen, J. G. *Appl. Catal. A Gen.* **2007**, *333*, 254–263.

(14) McCue, A. J.; McRitchie, C. J.; Shepherd, A. M.; Anderson, J. A. *J. Catal.* **2014**, *319*, 127–135.

(15) McCue, A. J.; Shepherd, A. M.; Anderson, J. A. *Catal. Sci. Technol.* **2015**, *5*, 2880–2890.

(16) Sheth, P. A.; Neurock, M.; Smith, C. M. *J. Phys. Chem. B* **2005**, *109*, 12449–12466.

(17) Zhao, Z.; Zhao, J.; Chang, X.; Zha, S.; Zeng, L.; Gong, J. *AIChE J.* **2018**, *65*, 1059–1066.

(18) Tsapina, A. M.; Tsyrulnikov, P. G.; Glyzdova, D. V.; Shlyapin, D. A.; Vedyagin, A. A.; Kaichev, V. V.; Trenikhin, M. V.; Trigub, A. L.; Lavrenov, A. V. *Appl. Catal. A Gen.* **2018**, *563*, 18–27.

(19) Leviness, S.; Nair, V.; Weiss, A. H.; Schay, Z.; Guczi, L. *J. Mol. Catal.* **1984**, *25*, 131–140.

(20) Mccue, A. J.; Mcritchie, C. J.; Shepherd, A. M.; Anderson, J. A. *J. Catal.* **2014**, *319*, 127–135.

(21) Feng, Q.; Zhao, S.; Wang, Y.; Dong, J.; Chen, W.; He, D.; Wang, D.; Yang, J.; Zhu, Y.; Zhu, H.; Gu, L.; Li, Z.; Liu, Y.; Yu, R.; Li, J.; Li, Y. *J. Am. Chem. Soc.* **2017**, *139*, 7294–7301.

(22) Studt, F.; Abild-Pedersen, F.; Bligaard, T.; Sorensen, R. Z.; Christensen, C. H.; Norskov, J. K. *Science (80-.).* **2008**, *320*, 1320–1322.

(23) Sheth, P. A.; Neurock, M.; Smith, C. M. *J. Phys. Chem. B* **2003**, *107*, 2009–2017.

(24) Gates, J. A.; Kesmodel, L. L. *J. Chem. Phys.* **1982**, *76*, 4281–4286.

(25) Kesmodel, L. L.; Gates, J. A. *J. Electron Spectros. Relat. Phenomena* **1983**, *29*, 307–312.

(26) Kesmodel, L. L.; Waddill, G. D.; Gates, J. A. *Surf. Sci.* **1984**, *138*, 464–474.

(27) Gates, J. A.; Kesmodel, L. L. *Surf. Sci. Lett.* **1982**, *120*, L461–L467.

(28) Ormerod, R. M.; Lambert, R. M.; Hoffmann, H.; Zaera, F.; Wang, L. P.; Bennett, D. W.;

Tysoe, W. T. *J. Phys. Chem.* **1994**, *98*, 2134–2138.

(29) Azad, S.; Kaltchev, M.; Stacchiola, D.; Wu, G.; Tysoe, W. T. *J. Phys. Chem. B* **2000**, *104*, 3107–3115.

(30) Clotet, A.; Ricart, J. M.; Pacchioni, G. *J. Mol. Struct. Theochem* **1998**, *458*, 123–129.

(31) Clotet, A.; Pacchioni, G. *Surf. Sci.* **1996**, *346*, 91–107.

(32) Krooswyk, J. D.; Waluyo, I.; Trenary, M. *ACS Catal.* **2015**, *5*, 4725–4733.

(33) Ball, M. R.; Rivera-Dones, K. R.; Stangland, E.; Mavrikakis, M.; Dumesic, J. A. *J. Catal.* **2019**, *370*, 241–250.

(34) Ruban, A. V.; Skriver, H. L.; Nørskov, J. K. *Phys. Rev. B - Condens. Matter Mater. Phys.* **1999**, *59*, 15990–16000.

(35) Seemala, B.; Cai, C. M.; Wyman, C. E.; Christopher, P. *ACS Catal.* **2017**, *7*, 4070–4082.

(36) Xu, C. Q.; Lee, M. S.; Wang, Y. G.; Cantu, D. C.; Li, J.; Glezakou, V. A.; Rousseau, R. *ACS Nano* **2017**, *11*, 1649–1658.

(37) Tauster, S. J.; Fung, S. C.; Garten, R. L. *J. Am. Chem. Soc.* **1978**, *100*, 170–175.

(38) Kang, J. H.; Shin, E. W.; Kim, W. J.; Park, J. D.; Moon, S. H. *J. Catal.* **2002**, *208*, 310–320.

(39) Ro, I.; Sener, C.; Stadelman, T. M.; Ball, M. R.; Venegas, J. M.; Burt, S. P.; Hermans, I.; Dumesic, J. A.; Huber, G. W. *J. Catal.* **2016**.

(40) Xu, X.; Goodman, D. W. *J. Phys. Chem.* **2005**, *97*, 683–689.

(41) Hadjiivanov, K.; Kno, H. *J. Phys. Chem. B* **1998**, *102*, 10936–10940.

(42) Rebelli, J.; Rodriguez, A. A.; Ma, S.; Williams, C. T.; Monnier, J. R. *Catal. Today* **2011**, *160*, 170–178.

(43) Gao, F.; Goodman, D. W. *Chem. Soc. Rev.* **2012**, *41*, 8009.

(44) Giorgi, J. B.; Schroeder, T.; Bäumer, M.; Freund, H.-J. *Surf. Sci.* **2002**, *498*, L71–L77.

(45) Yudanov, I. V.; Sahnoun, R.; Neyman, K. M.; Rösch, N.; Hoffmann, J.; Schauermann, S.; Johánek, V.; Unterhalt, H.; Rupprechter, G.; Libuda, J.; Freund, H. J. *J. Phys. Chem. B* **2003**, *107*, 255–264.

(46) Loffreda, D.; Simon, D.; Sautet, P. *Surf. Sci.* **1999**, *425*, 68–80.

(47) Primet, M.; Mathieu, M. V.; Sachtler, W. M. H. *J. Catal.* **1976**, *44*, 324–327.

(48) Sakong, S.; Mosch, C.; Groß, A. *Phys. Chem. Chem. Phys.* **2007**, *9*, 2216–2225.

(49) Xu, L.; Stangland, E. E.; Mavrikakis, M. *J. Catal.* **2018**, *362*, 18–24.

(50) Hill, J. M.; Shen, J.; Watwe, R. M.; Dumesic, J. A. *Langmuir* **2000**, *16*, 2213–2219.

(51) Sheppard, N.; De La Cruz, C. *Adv. Catal.* **1996**, *41*, 1–112.

(52) Mei, D.; Sheth, P.; Neurock, M.; Smith, C. *J. Catal.* **2006**, *242*, 1–15.

(53) Beebe, T. P.; Yates, J. T. *J. Phys. Chem.* **2005**, *91*, 254–257.

(54) Liu, Y.; He, Y.; Zhou, D.; Feng, J.; Li, D. *Catal. Sci. Technol.* **2016**, *6*, 3027–3037.

(55) Borodziński, A.; Gołębiowski, A. *Langmuir* **1997**, *13*, 883–887.

(56) McLeod, A. S.; Blackwell, R. *Chem. Eng. Sci.* **2004**, *59*, 4715–4721.

(57) Borodziński, A.; Cybulski, A. *Appl. Catal. A Gen.* **2000**, *198*, 51–66.

(58) Benavidez, A. D.; Burton, P. D.; Nogales, J. L.; Jenkins, A. R.; Ivanov, S. A.; Miller, J. T.; Karim, A. M.; Datye, A. K. *Appl. Catal. A Gen.* **2014**, *482*, 108–115.

(59) Vignola, E.; Steinmann, S. N.; Al Farra, A.; Vandegehuchte, B. D.; Curulla, D.; Sautet, P. *ACS Catal.* **2018**, *8*, 1662–1671.

(60) Takht Ravanchi, M.; Sahebdelfar, S. *Appl. Catal. A Gen.* **2016**, *525*, 197–203.

(61) Sárkány, A. *React. Kinet. Catal. Lett.* **2001**, *74*, 299–307.

(62) González, C. A.; Bartoszek, M.; Martin, A.; De Correa, C. M. *Ind. Eng. Chem. Res.* **2009**, *48*, 2826–2835.

(63) Babu, N. S.; Lingaiah, N.; Pasha, N.; Kumar, J. V.; Prasad, P. S. S. *Catal. Today* **2009**, *141*, 120–124.

(64) Liu, Y.; Zhao, J.; He, Y.; Feng, J.; Wu, T.; Li, D. *J. Catal.* **2017**, *348*, 135–145.

(65) He, Y.; Fan, J.; Feng, J.; Luo, C.; Yang, P.; Li, D. *J. Catal.* **2015**, *331*, 118–127.

(66) Wang, S.; Zhao, G.; Liu, Y.; Lu, Y. *Ind. Eng. Chem. Res.* **2019**, *58*, 16431–16441.

(67) McCue, A. J.; Anderson, J. A. *J. Catal.* **2015**, *329*, 538–546.

(68) Pei, G.; Liu, X.; Chai, M.; Wang, A.; Zhang, T. *Cuihua Xuebao/Chinese J. Catal.* **2017**, *38*, 1540–1548.

(69) Molero, H.; Bartlett, B. F.; Tysoe, W. T. *J. Catal.* **1999**, *181*, 49–56.

(70) Ro, I.; Liu, Y.; Ball, M. R.; Jackson, D. H. K.; Chada, J. P.; Sener, C.; Kuech, T. F.; Madon, R. J.; Huber, G. W.; Dumesic, J. A. *ACS Catal.* **2016**, *6*, 7040–7050.

(71) Aragão, I. B.; Ro, I.; Liu, Y.; Ball, M.; Huber, G. W.; Zanchet, D. *Appl. Catal. B Environ.* **2018**, *222*, 1–2.

(72) Sener, C.; Wesley, T. S.; Alba-Rubio, A. C.; Kumbhalkar, M. D.; Hakim, S. H.; Ribeiro, F. H.; Miller, J. T.; Dumesic, J. A. *ACS Catal.* **2016**, *6*, 1334–1344.

(73) Hakim, S. H.; Sener, C.; Alba-Rubio, A. C.; Gostanian, T. M.; O'Neill, B. J.; Ribeiro, F. H.; Miller, J. T.; Dumesic, J. A. *J. Catal.* **2015**, *328*, 75–90.

(74) Liu, Y.; Göeltl, F.; Ro, I.; Ball, M. R.; Sener, C.; Aragão, I. B.; Zanchet, D.; Huber, G. W.; Mavrikakis, M.; Dumesic, J. A. *ACS Catal.* **2017**, *7*, 4550–4563.

(75) Seyedmonir, S. R.; Strohmayer, D. E.; Geoffroy, G. L.; Vannice, M. A.; Young, H. W.; Linowski, J. W. *J. Catal.* **1984**, *87*, 424–436.

(76) Evans, J. W. W.; Wainwright, M. S. S.; Bridgewater, A. J. J.; Young, D. J. J. *Appl. Catal.* **1983**, *7*, 75–83.

(77) Shen, J.; Hill, J. M.; Watwe, R. M.; Spiewak, B. E.; Dumesic, J. A. *J. Phys. Chem. B* **1999**, *103*, 3923–3934.

(78) Carrasquillo-Flores, R.; Ro, I.; Kumbhalkar, M. D.; Burt, S.; Carrero, C. A.; Alba-Rubio, A. C.; Miller, J. T.; Hermans, I.; Huber, G. W.; Dumesic, J. A. *J. Am. Chem. Soc.* **2015**, *137*, 10317–10325.

Table of Contents Figure